Title

Giant phytoplankton revealed by in situ imaging

Journal

Limnology and Oceanography Letters, 11(5)

ISSN

2378-2242

Authors

Ohman, Mark D

Leblanc, Karine

Ellen, Jeffrey S

et al.

Publication Date

2026-09-01

DOI

10.1002/lol2.70163

LIMNOLOGY and OCEANOGRAPHY LETTERS

ASLO

Open Access

Limnology and Oceanography Letters 11, 2026, e70163

doi: 10.1002/lol2.70163

LETTER

Giant phytoplankton revealed by in situ imaging

Mark D. Ohman [1]* **Karine Leblanc** [2] **Jeffrey S. Ellen** [1,3] **Sven Gastauer** [1,4]

[1]Integrative Oceanography Division, Scripps Institution of Oceanography, University of California San Diego, La Jolla, California, USA; [2]Aix-Marseille Université, Université de Toulon, CNRS, IRD, MIO, Marseille, France; [3]Ulysses Maritime Technologies Inc., San Francisco, California, USA; [4]Thünen Institute of Sea Fisheries, Bremerhaven, Germany

Scientific Significance Statement

The size distribution of diatoms and other phytoplankton influences their accessibility to planktonic grazers, sinking velocities, and contributions to vertical export of biogenic elements, yet conventional methods remove phytoplankton from the ocean and lakes for measurement, often disrupting fragile chains and altering their natural morphology. One solution is to characterize undisturbed phytoplankton while suspended in their natural environment. Analysis of in situ images acquired with an autonomous *Zooglider* equipped with a flow-through imaging system that minimizes turbulence uncovered surprisingly long chains of diatoms and other phytoplankton, revealing elongate chains that are largely inaccessible to planktonic grazers and have the potential to sink rapidly through the ocean water column.

Abstract

Deployment of an autonomous *Zooglider* in the western Mediterranean Sea revealed the presence of long phytoplankton chains attaining maximum lengths of 6.4–10.4 mm suspended in situ. Elongate chains included the diatoms *Guinardia*, *Proboscia*, two other diatom morphologies, and solitary filaments of the cyanobacterium *Trichodesmium*. Most elongate chains were distributed in the upper 100 m of the water column, overlapping the deep chlorophyll maximum, but some extended to depths of 400 m, suggesting occasional export into deep waters. Such elongate chains appear to be an unutilizable prey resource for most mesozooplankton grazers, including planktonic copepods and appendicularians. Elongate chains are likely to be widely distributed in the ocean, but their detection requires noninvasive measurement methods that do not disrupt the fluid environment or disturb suspended phytoplankton.

Marine diatoms are fundamental constituents of pelagic food webs, influencing global primary production, food web transfers, particle export, and the cycling of C, Si, Fe, and other elements. Diatoms are commonly assumed to be of a size accessible to most grazing mesozooplankton, facilitating efficient trophic transfer and secondary production. While the overall size range of diatoms is ~ 2 μm to 2 mm (Halse and Syvertsen 1996), with occasional exceptions to 2–3 mm for the centric *Ethmodiscus* (Round et al. 1990) and even 4 mm for the pennate *Thalassiothrix antarctica* (Quilty et al. 1985; Smetacek 2000), single-cell diatoms more typically range from 10 to 200 μm. When pelagic food webs are represented as size spectra, diatoms are often categorized in size bins of ~ 3 to 100 μm (e.g., Mattern et al. 2026).

*Correspondence: mohman@ucsd.edu

Associate editor: Dongyan Liu

Diatoms suspended in the form of aggregated elongate mats have been found in different ocean basins, with mats of *Rhizosolenia* spp. and other taxa averaging ~ 40 mm, extending up to 300 mm in diameter (Carpenter et al. 1977; Villareal et al. 1993, 1999). However, their constituent cells and chains rarely exceed 2 mm (Villareal et al. 1993) or 3–4 mm (*Thalassiothrix antarctica*, Quilty et al. 1985, Smetacek 2000). The largest diatom chains are found in the Arctic sea ice flora, where *Melosira arctica* form long ribbons hanging several meters from the ice (Poulin et al. 2014).

Accurate representation of the size composition of cells and chains is important for diverse issues in aquatic ecology. Phytoplankton-grazer interactions often are described as size-dependent, with both metazoan and protistan zooplankton ingesting a limited part of the size spectrum of available cells (Kiørboe 2008). Size is not the only criterion for ingestion, as siliceous setae and colony formation (Pančić and Kiørboe 2018), mechanically resistant frustules (Hamm et al. 2003), and chemical defenses (Ianora and Miralto 2010) can alter the edibility of diatoms. Size also influences cell sinking velocities, hence export potential out of the euphotic zone. The extent to which food webs and export potential can be accurately characterized by size spectra (e.g., Serra-Pompei et al. 2022; Stukel et al. 2024) also depends on appropriate representation of the size range of these organisms.

Common methods for characterizing the size composition of diatoms and other phytoplankton disturb filaments before measurement. Collection by plankton nets, water bottles, pumps, and traps risks mechanical damage. Even entrapment in water bottles typically involves flow through collecting tubing, funnels, or other concentrating devices that alter the flow regime and introduce surfaces for contact. Peperzak et al. (2003) noted "Although sampling and sample handling were performed carefully, chains and phytoplankton aggregates may have broken up to an unknown extent." Chemical fixation introduces further distortions of natural cell and chain morphology.

In situ imaging is an alternative for characterizing fragile suspended planktonic organisms (Lombard et al. 2019). However, most imaging devices are mounted on surface-tethered instruments like a CTD-rosette, where mechanically coupled motions induce fluid flow capable of disrupting chains and cells. Mounting an imaging device on an ocean glider, where the glider hull has been carefully engineered to reduce drag and minimize flow discontinuities, mitigates these disruptions (e.g., Ohman et al. 2018; Picheral et al. 2022). Extremely long phytoplankton filaments (to 22 mm) were reported from *Zooglider* deployments in the California Current System (Ohman 2019), although one chain in figure one of that publication was erroneously referred to as a diatom, when it is a filament of *Trichodesmium*.

Here we report on elongate "giant" diatom chains and cyanobacteria filaments suspended in the water column of the western Mediterranean Sea. We define "giant" phytoplankton as chains of extraordinary size, exceeding by an order of magnitude the general expectations of chains smaller than 200 μm. The chains we documented were imaged in situ by an autonomous *Zooglider* and attained lengths of 6.4–10.4 mm. Accompanying shipboard collections of phytoplankton illustrated the diversity of diatom and cyanobacteria found in the water column. We explore some of the implications of more accurately characterizing phytoplankton size composition in situ, including the relative inaccessibility of elongate chains to most zooplankton grazers and implications for vertical C export.

Methods

Zooglider was deployed in the western Mediterranean Sea between March 20–May 8, 2023 as a part of the BioSWOT-Med program (Doglioli and Grégori 2023; Doglioli et al. 2024). It was initially released off the coast of Majorca, Spain, navigated to south of Menorca, then recovered at sea and redeployed in the center of an anticyclonic eddy north of Menorca (Fig. 1). The shadowgraph imaging Zoocam on *Zooglider* was activated for dives 1–8 (Majorca, 30 March), dives 245–314 (south of Menorca, April 24–May 3), and dives 353–389 (eddy, May 4–8). During intervening dives the Zoocam was powered off to conserve memory. During each dive science instruments were powered off during *Zooglider* descent, while biowipers and a UV-LED were activated to eliminate biofouling and onboard computations were carried out. Instruments (Zoocam, Zonar, pumped Seabird CP141 CTD, and SeaPoint mini-SCF chlorophyll *a* fluorometer) were then activated during ascent from approximately 420 m to the sea surface. A summary data stream was telemetered ashore via Iridium upon each surfacing. *Zooglider* ascended at ~ 10 cm s^{-1} and the Zoocam sampled at 1 Hz throughout ascent, providing an image approximately every 10 cm of vertical travel. The 15 cm light path of the Zoocam is illuminated with a red LED (620–630 nm), imaging 250 mL per frame. Shadowgraph imaging with a telecentric lens permits objects to be measured accurately, independent of their axial position in the light beam. Further details are in Ohman et al. (2018).

After flatfielding, regions of interest were segmented using a two-step Canny edge detector (Ellen 2018; Ohman et al. 2018). Regions of interest were pre-classified using a convolutional neural network (Ellen and Ohman 2024), then the classification of regions of interest manually verified. In this verification process we observed numerous phytoplankton chains whose morphology was familiar, but whose dimensions were much greater than expected. We therefore retrieved a subset of phytoplankton chains whose feret diameter was ≥ 2 mm for closer manual inspection. These regions of interest were measured manually with an on-screen digital tool.

Zoocam was originally designed to image mesozooplankton between 0.5 and 20 mm, but does not sufficiently resolve most phytoplankton. The pixel size is 40 μm, which is too

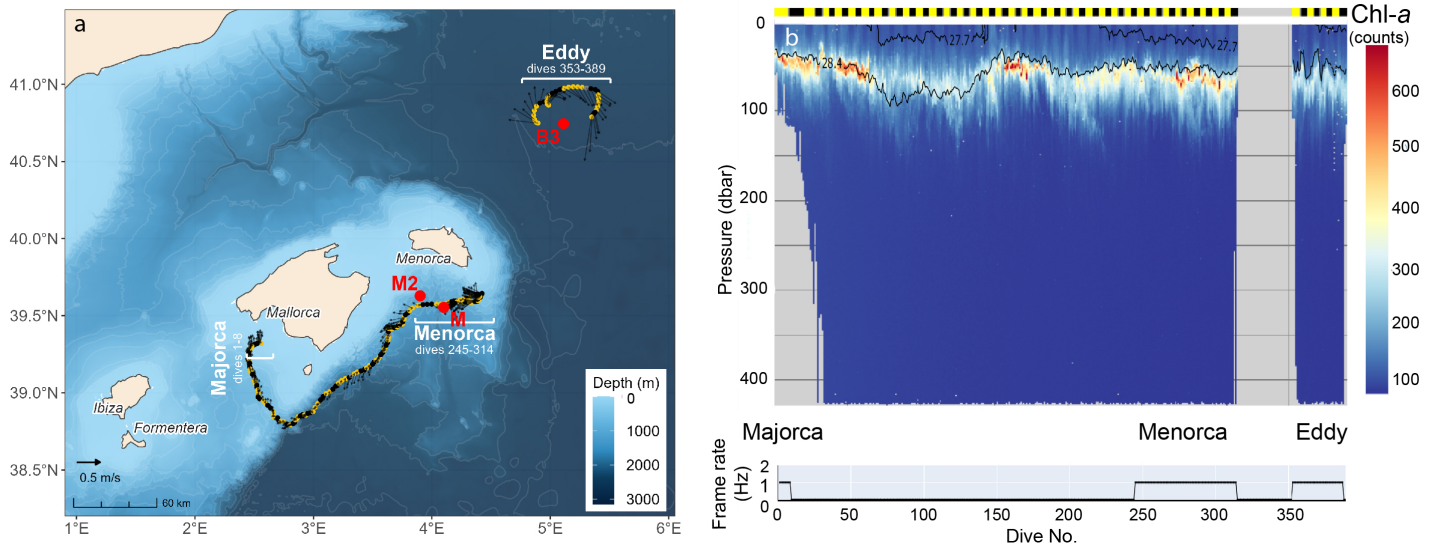

Fig. 1. *Zooglider* trajectory in the western Mediterranean Sea in conjunction with the BioSWOT-Med cruise, March 30–May 8, 2023. (**a**) *Zooglider* track with dive numbers indicating dives when Zoocam was activated in three regions. Day/night coded yellow/black; black vectors indicate water column-averaged current velocity. Letters M, M2, and B3 indicate shipboard water column sampling locations. (**b**) Vertical section of along-track chlorophyll *a* fluorescence (contours indicate σ_θ). Day/night coded yellow/black. Lower panel indicates dives when Zoocam was activated, at 1 Hz. Gray gap indicates when *Zooglider* was transported aboard ship. Concentrations of extracted chlorophyll *a* + phaeopigments from shipboard samples (*Y*, mg pigments L^{-1}) were related to concurrent measures of in vivo fluorescence by *Zooglider* (*X*, counts) ($r^2 = 0.50$, $p < 10^{-14}$, $Y = 0.0037X - 0.189$).

large to resolve frustule and cellular structure or other morphological details that are typically necessary to identify cells. However, five major groups of elongate chains were resolvable throughout this *Zooglider* mission and are discussed herein.

During BioSWOT-Med, vertical phytonet hauls were performed from the RV *L'Atalante* at three locations near water parcels sampled by *Zooglider*, two south of Menorca (Stas. M, M2) and one in the eddy (Sta. B3; Fig. 1a; Supporting Information Table S1). The sampling/sensing events were displaced somewhat in time (minimum 0.6–103 h) and space (17–28 km), because they were not designed to be synchronized, but both sampled the same water masses and presumably similar plankton communities. Each haul was from 0 to 150 m with a 20 μm mesh net. Net collector contents were passed gently through a 2 mm mesh sieve, then diluted to 1 L with filtered seawater. Two samples (60 mL) were fixed with acidified Lugols solution and buffered formaldehyde for light microscopy observations. One milliliter of the fresh net material was filtered onboard without fixative at low vacuum onto a 25 mm polycarbonate membrane and rinsed with MilliQ water, dried for 3 h at 50°C, then kept at room temperature for subsequent SEM analyses. Phytoplankton diversity was assessed by cell counts in light microscopy (Nikon TE200) while SEM samples were gold coated and analyzed on a Phenom ProX benchtop SEM.

Data and metadata are available at Ohman et al. (2026).

Results

Chlorophyll-*a* along the glider track (Fig. 1a) showed a persistent deep chlorophyll maximum layer at approximately 45–75 m depth, with lower concentrations in the eddy (Fig. 1b). Most of the spatial variability in depth was explained by vertical deflections of isopycnal surfaces (Fig. 1b).

Zoocam images from all three regions (Majorca, Menorca, and Eddy) revealed chains of diverse phytoplankton significantly longer than previously reported (Fig. 2; Supporting Information Figs. S1–S5). Most of the phytoplankton chains were not identifiable to genus, but some distinctive morphologies were recognizable, including helically coiled *Guinardia* spp. (Fig. 2a), chains of *Proboscia* spp. (Fig. 2b), other diatom chains whose constituent cells had similar length and width dimensions (Fig. 2c), diatom chains with cells much longer than wide (Fig. 2d), and individual filaments of the cyanobacteria *Trichodesmium* (Fig. 2e). The surprising characteristic of these chains was their length, with maxima of 10.43, 9.94, 6.41, 7.37, and 9.68 mm for these five categories of chains, respectively (Table 1). Mean chain lengths were 3.8–5.3 mm for these categories (Table 1, Supporting Information Fig. S6).

Microscopic examination of preserved phytoplankton samples revealed 88 taxa of diatoms plus numerous other cell types (complete floristic analysis to be presented in Leblanc et al. in preparation). Among identified taxa, a variety of larger chain-forming phytoplankton, including diatoms and *Trichodesmium*, were present (Table S2). Some large dinoflagellates (e.g., *Pyrocycstis* and *Ceratium fusus*) were

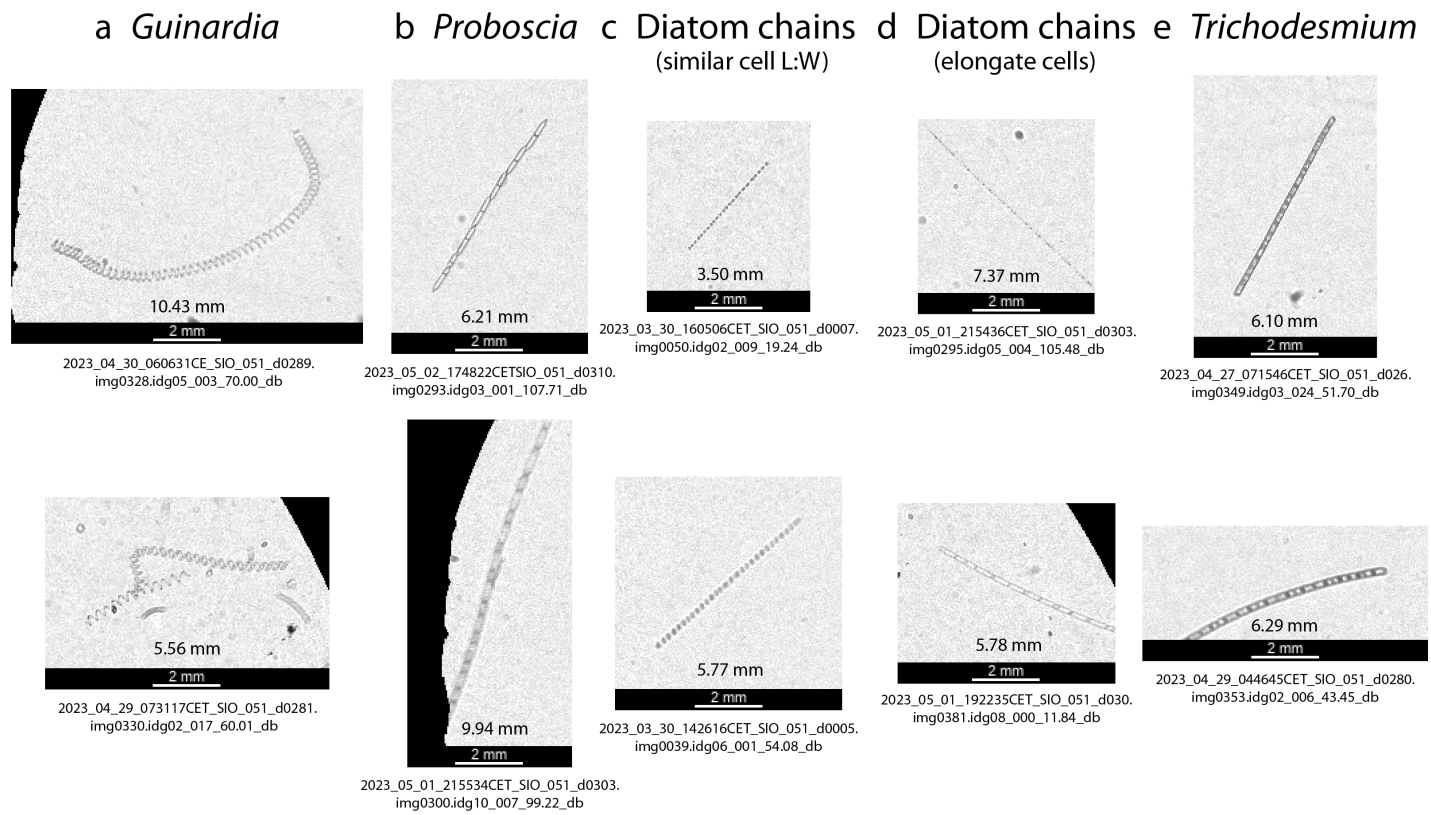

Fig. 2. Representative examples of elongate phytoplankton chains imaged in situ in the BioSWOT-Med region. Chains of: (**a**) the diatom *Guinardia* spp., (**b**) the diatom *Proboscia* spp., (**c**) diatom chains with similar length : width ratio of individual cells, (**d**) diatom chains with individual cell length much greater than width, (**e**) elongate filaments of the cyanobacterium *Trichodesmium* spp. Hand-measured length (in mm) on each image. Image metadata are indicated beneath each image (date, local time, mission number, dive number, image number, sampling depth as pressure in dbar).

Table 1. Lengths of phytoplankton chains imaged in situ by the shadowgraph Zoocam on *Zooglider*.

Chain morphology	Maximum length (mm)	Mean length ± 95% (mm)	*N*
Guinardia (spiral chains)	10.43	4.19 ± 0.44	64
Prosboscia	9.94	4.78 ± 1.94	8
Diatom chains (similar cell L:W)	6.41	3.82 ± 0.12	164
Diatom chains (elongate cells)	7.37	5.26 ± 0.74	14
Trichodesmium	9.68	5.34 ± 0.96	16

detected. A few of the numerically dominant larger chains at Stas. M and/or M2, south of Menorca, included *Stephanopyxis* cf. *palmeriana, Chaetoceros* spp., *Hemiaulus hauckii*, *Thalassiothrix* spp., *Thalassionema* spp., *Rhizosolenia styliformis*, *Pseudosolenia calcar-avis*, *Pseudo-nitzschia* spp., *Proboscia* spp., *Trichodesmium* spp., and others. At Sta. B3, in the eddy, many of the same taxa were found, plus *Leptocylindrus mediterraneus*, *Guinardia* spp., and *Bacteriastrum* spp. Hence, the phytoplankton morphologies recognized by *Zooglider* were also reflected in the independent phytoplankton samples. For the five major groups identified in *Zooglider* images, the longest in situ imaged chains were consistently longer than corresponding types of phytoplankton collected and analyzed by microscopy (Supporting Information Table S2 and Fig. S6).

The spatial distribution of large chains (Fig. 3) showed varying degrees of overlap with the depth of the deep chlorophyll maximum layer (Fig. 1b), especially for *Guinardia*, *Proboscia*, diatom chains with elongate individual cells, and filaments of *Trichodesmium*. We assume the absence of the last three categories of chains south of Majorca does not reflect true zeroes, but only abundances below detection limits. In contrast, diatom chains having cells with similar cell lengths and widths extended through a much broader sector of the water column (Fig. 3e). The latter chains extended from the surface to 83 m south of Majorca (maximum depth sampled there), from 0 to 260 m south of Menorca, and from 0 to 397 m in the anticyclonic eddy. In the latter case, chains were observed on multiple dives at

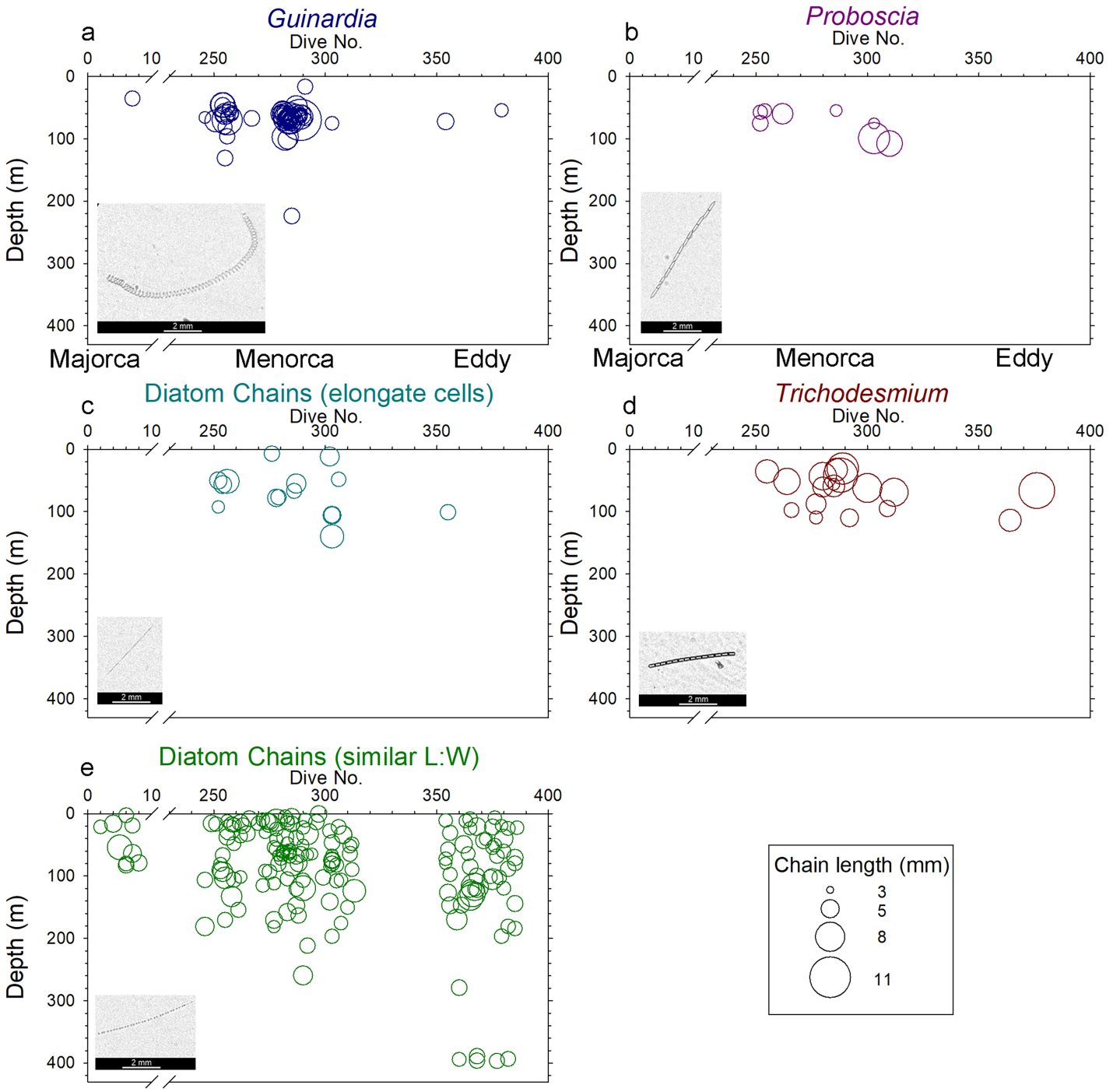

Fig. 3. Vertical sections illustrating occurrence of elongate phytoplankton along the *Zooglider* trajectory. (**a**) Spiral chains of the diatom *Guinardia* spp., (**b**) chains of the diatom *Proboscia* spp., (**c**) diatom chains with individual cell length much greater than width, (**d**) elongate filaments of the cyanobacterium *Trichodesmium* spp., and (**e**) diatom chains with similar length : width ratio of individual cells. The diameter of each circle is proportional to chain length (in millimeters).

depths far below the euphotic zone, near the maximum depth sampled by *Zooglider*.

An example of the unsuitability of such exceptionally long chains for planktonic grazers is seen in Fig. 4, where two zooplankters are imaged in a frame with a few hundred phytoplankton chains, at 75.03 dbar. The appendicularian in the right side of the frame (*Oikopleura* sp.) secretes a mucus house with a complex of filters (Flood and Deibel 1998; Gorsky and

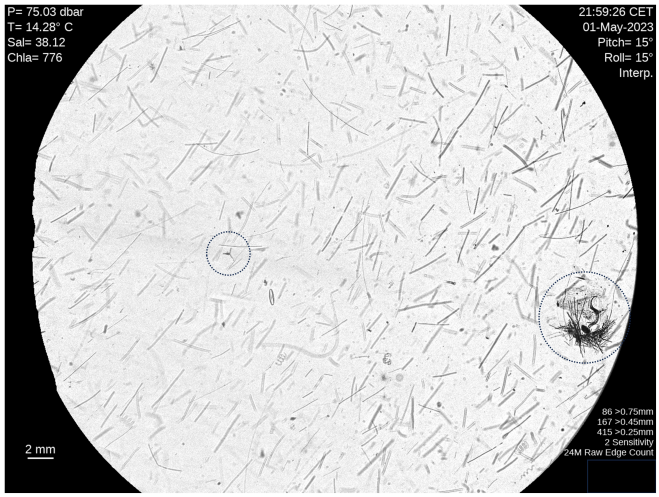

Fig. 4. Zoocam full frame image at a pressure of 75.03 dbar from dive 303, illustrating numerous elongate phytoplankton chains. Note encircled *Oithona* (copepod) at left and *Oikopleura* sp. (appendicularian) at right with incurrent filters of mucus house clogged with diatom chains.

Fenaux 1998). The coarse-mesh incurrent filters on the animal's house are clogged with numerous diatom chains that cannot be ingested. Encircled in the same image is a common planktonic copepod (*Oithona* sp.), whose body dimensions are much smaller than nearly all the phytoplankton chains visible in the image. Such phytoplankton chains are unlikely to be ingested and utilized by these and many other mesozooplankton taxa, despite their relatively high concentrations.

Discussion

Throughout our study region in the western Mediterranean Sea we imaged phytoplankton chains in situ that are considerably longer than those sampled by conventional approaches and commonly reported in the literature. These phytoplankton include chains of diatoms and the diazotroph *Trichodesmium* sp. Sampling confirmed that the cell morphologies we imaged are present in plankton samples, but at much smaller chain lengths. This suggests that conventional net tows (and probably sampling by water bottles and pumps) disrupt and fragment chains, shifting phytoplankton size distributions to much smaller apparent sizes than occur when suspended naturally in the water column. Although our phytoplankton samples had been passed through a 2-mm mesh, neither a previous analysis of net-collected phytoplankton in this region (Crombet et al. 2011, no pre-screening through a mesh) nor multiple years of microscopic analysis of coastal waters in this region have ever detected such long chains by microscopy (Karine Leblanc, personal observation).

Apart from large mats of aggregated diatoms such as *Rhizosolenia* noted above, elongate diatoms have been observed previously as either solitary cells (*Ethmodiscus rex*; McHugh 1954) or individual chains (Ohman 2019) in the California Current System, in the North Pacific Central Gyre (Villareal et al. 2007), and elsewhere. In a Pacific fjord, diatom chains to 8 mm were imaged by a holographic camera (Talapatra et al. 2013). On the Kerguelen Plateau in the Southern Ocean, chains of the colonial diatom *Corethron inerme* were observed in bottlenet samples (gentler handling than phytonets) to 7–8 mm length (Leblanc et al. 2021). Birocchi et al. (2026) reported elongate diatoms imaged in a tropical estuary. Their illustrations depict chains up to 2.2 mm in length, as well as helically coiled *Guinardia striata* chains of very similar morphology to our *Guinardia* chains, in their case to 1.2 mm long. We suspect that elongate diatoms are widespread in the ocean, and will become detectable with the use of other noninvasive sampling approaches that do not disturb suspended phytoplankton.

We focused our analysis on phytoplankton chains > 2 mm to screen for the largest chain morphologies present in our images. Many additional chains were smaller than 2 mm, representing a major additional compartment of living diatoms that are also likely to be of variable accessibility to the rest of the food web. However, we cannot presently assess the quantitative importance of elongate chains relative to smaller, more conventionally measured phytoplankton because our Zoocam was designed to record images of organisms > 0.45 mm. Subsequent studies should explicitly design sampling across the entire size spectrum of phytoplankton (using a combination of noninvasive in situ imaging, imaging flow cytometry or microscopy, and standard flow cytometry) in order to resolve the quantitative contribution that these giant phytoplankton make to C biomass and food web processes. We caution that the collection and processing of samples for imaging flow cytometry is likely to exclude or damage the largest chains, similar to what we document here.

We have confirmed the reliability of Zoocam length measurements when imaging objects of known size (Ohman et al. 2018). When bias occurs, it is attributable to the orientation of objects at angles other than 90° to the image plane, resulting in an underestimate of true object length. Hence, the true distribution of phytoplankton lengths in situ is somewhat understated here. We have not attempted to estimate cell widths because the size of a single pixel (40 μm) is larger than the dimensions of many diatom siliceous frustules. Shadowgraph imaging with a telecentric lens records changes in the index of refraction and we have found that such changes may be detectable even for cell structures that are smaller than a single pixel. This can lead to a "halo" effect that can make a structure appear wider than in reality, which would affect width, but with negligible effects on length measurements addressed here.

The existence of suspended phytoplankton cells much larger than measured previously has implications for grazing losses in pelagic food webs, the representation of pelagic food webs in terms of size spectra, and mass fluxes of C and Si to the seafloor. Most of the several-mm long chains we documented will be

inedible to most mesozooplankton. Two of the primary grazer-exclusion mechanisms are mentioned above: first, mucus net feeders like appendicularians and other pelagic tunicates (salps, doliolids, pyrosomes) will be unlikely to ingest these giant chains because of clogging of their feeding apparatus. Second, ubiquitous crustaceans like planktonic copepods that are dwarfed by these long chains probably cannot ingest them, because cell widths exceed the animals' mouth openings. The chopsticks method of chain ingestion (Alcaraz et al. 1980) will not be effective on such wide cells. It is possible that some much larger mesozooplankton like euphausiids can fragment such chains, as has been observed with marine snow (Dilling et al. 1998); however, this remains to be tested. Although copepods and euphausiids have been observed clinging to *Rhizosolenia* mats (Carpenter et al. 1977), and pelagic harpacticoid (but not calanoid or poecilostomatoid) copepods can ingest *Trichodesmium* (O'Neil and Roman 1994), in general the extremely long chain morphology observed here likely confers a strongly diminished rate of grazing mortality. Experimental work showing copepod clearance rates increasing with diatom chain length have been limited to chains < 0.2 mm (Kiørboe and Ryderheim 2026). It also seems unlikely that most protistan zooplankton would be able to effectively utilize such large prey items. Overall, the large size of these chains represents an effective deterrent to most grazing zooplankton (Bergkvist et al. 2012), but long chain breaking resistance has also been linked to nutrient status and likely results from the balance between growth and mechanical breakage by grazers and hydrodynamic forces (Young et al. 2012).

Representation of pelagic food webs as normalized size spectra has been adopted as a means to simplify food web structure (e.g., Serra-Pompei et al. 2022). However, a major increase in chain length implies a commensurate biovolume increase (assuming cylindrical geometry), which could call into question the log-linear spectral slopes that are often computed.

Our observations of diatom chains at depths as great as 400 m suggest that vertical export into deep waters may sometimes occur. In situ vertical velocities of chain-forming phytoplankton are uncertain and variable. Chains can remain neutrally buoyant for extended periods, sink rapidly in mass dump events (Alldredge and Gotschalk 1989; Kemp et al. 2000, 2006; Kemp and Villareal 2018), or diatom mats can also regulate buoyancy and rise through the water column after harvesting nutrients at depth (e.g., Villareal et al. 1993, 1999). While Stokes' law is often used to estimate phytoplankton sinking velocities, it was devised for spherical particles at low Reynolds number. Efforts have been made to modify Stokes' law to incorporate form resistance generated by elongate chains and other non-spherical particle shapes (e.g., Padisák et al. 2003). To consider sinking speeds of chains of 10 mm, in contrast with more conventionally measured dimensions of 1 or 0.1 mm, we consider a highly simplified case of diatoms with constant cell density of 1100 kg m^{-3} suspended in a fluid of density 1027 kg m^{-3}. Following Padisák et al. (2003), we apply a shape factor that slows diatom chain sinking speeds due to form resistance. Even considering increased form drag conferred by elongate chains in relation to spherical cells, a 1-mm chain would be expected to sink an order of magnitude faster than the same chain at a size of 0.1 mm. A 10 mm chain could sink 3 orders of magnitude faster than a 0.1 mm chain. The occurrence of most long diatom chains between 0 and 100 m depth in this study site suggests that these elongate chains are often not sinking, but regulating buoyancy to remain in the euphotic zone. However, under conditions of senescence or other stresses they may sink rapidly, potentially accelerating vertical transport of a variety of biogenic elements. We note that we detected the deepest chains in an anticyclonic eddy where vertical velocities of the fluid could further facilitate downward displacement and concentration (cf., Waite et al. 2016).

In sum, we conclude that the size composition of naturally occurring phytoplankton may historically have been severely biased because of artifacts associated with collecting, filtering, and preserving these fragile cells and chains. In situ imaging within an undisturbed fluid milieu reveals phytoplankton chain morphologies considerably longer than measurements obtained through conventional collection and preservation. Such elongate chains have implications for grazer deterrence, the size spectral composition of pelagic food webs, and the potential vertical export of biogenic elements.

Author Contributions

Mark D. Ohman and Sven Gastauer designed the *Zooglider* study and carried out data analysis. Karine Leblanc conducted taxonomic analysis of the phytoplankton. Jeffrey S. Ellen wrote code for image processing and carried out machine learning image classifications. All participated in the drafting and editing of the manuscript.

Acknowledgments

We express particular thanks to Andréa Doglioli and Gérald Grégori, MIO, Aix-Marseille Université for their leadership as Chief Scientists of the BioSWOT-Med cruise and for facilitating our participation in this research program. We appreciate scientific discussions with Francesco d'Ovidio, IPSL, Paris; Gaby Gorsky, LOV at Villefranche-sur-mer regarding the ecology of appendicularia; and Lee Karp-Boss, University of Maine, regarding phytoplankton sinking velocities. We thank the LOCEAN group, IPSL, Sorbonne University and Francesco d'Ovidio for accommodating Mark D. Ohman during manuscript preparation, and acknowledge the French state aid managed by the Agence Nationale de la Recherche under the "Investissements d'avenir" program, ANR-11-IDEX-0004-17-EURE-0006. We appreciate the financial support of the US National Science Foundation (OCE-2243190) for our *Zooglider* study, funding by the Gordon and Betty Moore Foundation for *Zooglider* development, and the overall support of BioSWOT-Med by the Agence Nationale de la

Recherche (ANR-23-CE01-0027). We thank Chris Wahl and Brent Jones (supported by TOSCA-CNES via BioSWOT-AdAC), as well as colleagues at SOCIB/IMEDEA, Spain, for *Zooglider* deployment. We thank the editor and reviewers for constructive comments on the manuscript. We dedicate this work to the late François Carlotti, whose scientific curiosity, analytical mind, and abiding friendship we always deeply appreciated.

Conflicts of Interest

None declared.

Data Availability Statement

Data and metadata from this study are freely available at the BCO-DMO data repository https://doi.org/10.26008/1912/BCO-DMO.999115.1.

References

Alcaraz, M., G. A. Paffenhofer, and J. R. Strickler. 1980. "Catching the Algae: A First Account of Visual Observations on Filter-Feeding Calanoids." In *Evolution and Ecology of Zooplankton Communities*, edited by W. C. Kerfoot, 241–248. University Press of New England.

Alldredge, A. L., and C. C. Gotschalk. 1989. "Direct Observations of the Mass Flocculation of Diatom Blooms—Characteristics, Settling Velocities and Formation of Diatom Aggregates." *Deep Sea Research Part A. Oceanographic Research Papers* 36, no. 2: 159–171. https://doi.org/10.1016/0198-0149(89)90131-3.

Bergkvist, J., P. Thor, H. H. Jakobsen, S. Wängberg, and E. Selander. 2012. "Grazer-Induced Chain Length Plasticity Reduces Grazing Risk in a Marine Diatom." *Limnology and Oceanography* 57, no. 1: 318–324. https://doi.org/10.4319/lo.2012.57.1.0318.

Birocchi, P., W. Oliveira-Souza, C. Braz, et al. 2026. "High-Resolution Temporal Dynamics of Diatoms in a Large and Well-Mixed Tropical Estuary." *Marine Environmental Research* 215: 107807. https://doi.org/10.1016/j.marenvres.2025.107807.

Carpenter, E. J., G. R. Harbison, L. P. Madin, et al. 1977. "*Rhizosolenia* mats." *Limnology and Oceanography* 22, no. 4: 739–741. https://doi.org/10.4319/lo.1977.22.1.0060.

Crombet, Y., K. Leblanc, B. Quéguiner, et al. 2011. "Deep Silicon Maxima in the Stratified Oligotrophic Mediterranean Sea." *Biogeosciences* 8, no. 2: 459–475. https://doi.org/10.5194/bg-8-459-2011.

Dilling, L., J. Wilson, D. Steinberg, and A. Alldredge. 1998. "Feeding by the Euphausiid *Euphausia pacifica* and the Copepod *Calanus pacificus* on Marine Snow." *Marine Ecology Progress Series* 170: 189–201. https://doi.org/10.3354/meps170189.

Doglioli, A., and G. Grégori. 2023. BioSWOT-Med cruise, RV L'Atalante https://doi.org/10.17600/18002392.

Doglioli, A. M., G. Grégori, F. D'Ovidio, et al. 2024. *BioSWOT Med. Biological Applications of the Satellite Surface Water and Ocean Topography in the Mediterranean. Ref. Rapport de Campagne*. Université Aix-Marseille. Archimer. Archive Institutionelle de l'IFREMER.

Ellen, J. S. 2018. "Improving Biological Object Classification in Plankton Images Using Convolutional Neural Networks." PhD Thesis, University of California, San Diego.

Ellen, J. S., and M. D. Ohman. 2024. "Beyond Transfer Learning: Leveraging Ancillary Images in Automated Classification of Plankton." *Limnology and Oceanography: Methods* 22, no. 12: 943–952. https://doi.org/10.1002/lom3.10648.

Flood, P. R., and D. Deibel. 1998. "The Appendicularian House." In *The Biology of Pelagic Tunicates*, edited by Q. Bone, 105–124. Oxford University Press.

Gorsky, G., and R. Fenaux. 1998. "The Role of Appendicularia in Marine Food Webs." In *The Biology of Pelagic Tunicates*, edited by Q. Bone, 161–169. Oxford University Press.

Halse, G. R., and E. E. Syvertsen. 1996. "Marine Diatoms." In *Identifying Marine Diatoms and Dinoflagellates*, edited by C. R. Tomas, 5–385. Academic Press.

Hamm, C. E., R. Merkel, O. Springer, et al. 2003. "Architecture and Material Properties of Diatom Shells Provide Effective Mechanical Protection." *Nature* 421, no. 6925: 841–843. https://doi.org/10.1038/nature01416.

Ianora, A., and A. Miralto. 2010. "Toxigenic Effects of Diatoms on Grazers, Phytoplankton and Other Microbes: A Review." *Ecotoxicology* 19, no. 3: 493–511. https://doi.org/10.1007/s10646-009-0434-y.

Kemp, A. E. S., R. B. Pearce, I. Grigorov, et al. 2006. "Production of Giant Marine Diatoms and their Export at Oceanic Frontal Zones: Implications for Si and C Flux from Stratified Oceans." *Global Biogeochemical Cycles* 20: Gb4s04. https://doi.org/10.1029/2006gb002698.

Kemp, A. E. S., J. Pike, R. B. Pearce, and C. B. Lange. 2000. "The "Fall Dump" – A New Perspective on the Role of a "Shade Flora" in the Annual Cycle of Diatom Production and Export Flux." *Deep-Sea Research Part II-Topical Studies in Oceanography* 47: 2129–2154. https://doi.org/10.1016/s0967-0645(00)00019-9.

Kemp, A. E. S., and T. A. Villareal. 2018. "The Case of the Diatoms and the Muddled Mandalas: Time to Recognize Diatom Adaptations to Stratified Waters." *Progress in Oceanography* 167: 138–149. https://doi.org/10.1016/j.pocean.2018.08.002.

Kiørboe, T. 2008. *A Mechanistic Approach to Plankton Ecology*. Princeton University Press.

Kiørboe, T., and F. Ryderheim. 2026. "Diatoms–Copepods: An Evolutionary Arms Race." *Limnology and Oceanography* 71, no. 4: e70355. https://doi.org/10.1002/lno.70355.

Leblanc, K., A. Lafond, V. Cornet, J. Legras, B. Marie, and B. Quéguiner. 2021. "Deep Particle Stocks Following the Summer Bloom around the Kerguelen Islands: Insights into Diatoms Physiological State, Community Structure and Mortality Modes." *Journal of Marine Systems* 222: 103609. https://doi.org/10.1016/j.jmarsys.2021.103609.

Lombard, F., E. Boss, A. M. Waite, et al. 2019. "Globally Consistent Quantitative Observations of Planktonic Ecosystems." *Frontiers in Marine Science* 6: 196. https://doi.org/10.3389/fmars.2019.00196.

Mattern, J. P., S. Dutkiewicz, J. E. Moscoso, and C. A. Edwards. 2026. "Zooplankton Grazing and Nutrient Supply Control the Emergence of Large Diatoms in Coastal Upwelling Systems: Insights from a Regional Ecosystem Model." *Limnology and Oceanography* 71, no. 2: e70332. https://doi.org/10.1002/lno.70332.

McHugh, J. L. 1954. "Distribution and Abundance of the Diatom *Ethmodiscus rex* off the West Coast of North America." *Deep-Sea Research* 1, no. 4: 216–223. https://doi.org/10.1016/0146-6313(54)90004-0.

Ohman, M. D. 2019. "A Sea of Tentacles: Optically Discernible Traits Resolved from Planktonic Organisms *In Situ*." *ICES Journal of Marine Science* 76, no. 7: 1959–1972. https://doi.org/10.1093/icesjms/fsz184.

Ohman, M. D., R. E. Davis, J. T. Sherman, et al. 2018. "*Zooglider*: An Autonomous Vehicle for Optical and Acoustic Sensing of Zooplankton." *Limnology and Oceanography: Methods* 17: 69–86. https://doi.org/10.1002/lom3.10301.

Ohman, M. D., K. Leblanc, J. S. Ellen, and S. Gastauer. 2026. *Large Phytoplankton Chain Lengths from BIOSWOT-Med Zooglider Deployment in the Northwest Mediterranean Sea during March to May 2023 (Version 1)*. Biological and Chemical Oceanography Data Management Office (BCO-DMO). https://doi.org/10.26008/1912/BCO-DMO.999115.1.

O'Neil, J. M., and M. R. Roman. 1994. "Ingestion of the Cyanobacterium *Trichodesmium* Spp. by Pelagic Harpacticoid Copepods *Macrosetella*, *Miracia* and *Oculosetella*." *Hydrobiologia* 292/293: 235–240. https://doi.org/10.1007/BF00229946.

Padisák, J., É. Soróczki-Pintér, and Z. Rezner. 2003. "Sinking Properties of some Phytoplankton Shapes and the Relation of Form Resistance to Morphological Diversity of Plankton: An Experimental Study." *Hydrobiologia* 500, no. 1–3: 243–257. https://doi.org/10.1023/a:1024613001147.

Pančić, M., and T. Kiørboe. 2018. "Phytoplankton Defence Mechanisms: Traits and Trade-Offs." *Biological Reviews of the Cambridge Philosophical Society* 93, no. 2: 1269–1303. https://doi.org/10.1111/brv.12395.

Peperzak, L., F. Colijn, R. Koeman, W. W. C. Gieskes, and J. C. A. Joordens. 2003. "Phytoplankton Sinking Rates in the Rhine Region of Freshwater Influence." *Journal of Plankton Research* 25, no. 4: 365–383. https://doi.org/10.1093/plankt/25.4.365.

Picheral, M., C. Catalano, D. Brousseau, et al. 2022. "The Underwater Vision Profiler 6: An Imaging Sensor of Particle Size Spectra and Plankton, for Autonomous and Cabled Platforms." *Limnology and Oceanography: Methods* 20, no. 2: 115–129. https://doi.org/10.1002/lom3.10475.

Poulin, M., G. J. C. Underwood, and C. Michel. 2014. "Sub-Ice Colonial *Melosira arctica* in Arctic First-Year Ice." *Diatom Research* 29, no. 2: 213–221. https://doi.org/10.1080/0269249x.2013.877085.

Quilty, P. G., K. R. Kerry, and H. J. Marchant. 1985. "A Seasonally Recurrent Patch of Antarctic Planktonic Diatoms." *Search* 16, no. 1–2: 48.

Round, F. E., R. M. Crawford, and D. G. Mann. 1990. *The Diatoms. Biology and Morphology of the Genera*, 747. Cambridge: Cambridge University Press.

Serra-Pompei, C., B. Ward, J. M. Pinti, A. W. Visser, T. Kiørboe, and K. H. Andersen. 2022. "Linking Plankton Size Spectra and Community Composition to Carbon Export and its Efficiency." *Global Biogeochemical Cycles* 36, no. 5: e2021GB007275. https://doi.org/10.1029/2021gb007275.

Smetacek, V. 2000. "Oceanography—The Giant Diatom Dump." *Nature* 406, no. 6796: 574–575. https://doi.org/10.1038/35020665.

Stukel, M. R., M. Décima, T. B. Kelly, et al. 2024. "Relationships Between Plankton Size Spectra, Net Primary Production, and the Biological Carbon Pump." *Global Biogeochemical Cycles* 38, no. 4: e2023GB007994. https://doi.org/10.1029/2023GB007994.

Talapatra, S., J. R. Hong, M. McFarland, et al. 2013. "Characterization of Biophysical Interactions in the Water Column Using In Situ Digital Holography." *Marine Ecology Progress Series* 473: 29–51. https://doi.org/10.3354/meps10049.

Villareal, T. A., M. A. Altabet, and K. Culver-Rymsza. 1993. "Nitrogen Transport by Vertically Migrating Diatom Mats in the North Pacific Ocean." *Nature* 363, no. 6431: 709–712. https://doi.org/10.1038/363709a0.

Villareal, T. A., R. M. L. McKay, M. M. D. Al-Rshaidat, R. Boyanapalli, and R. M. Sherrell. 2007. "Compositional and Fluorescence Characteristics of the Giant Diatom *Ethmodiscus* along a 3000 km Transect (28°N) in the Central North Pacific Gyre." *Deep Sea Research Part A. Oceanographic Research Papers* 54, no. 8: 1273–1288. https://doi.org/10.1016/j.dsr.2007.04.018.

Villareal, T. A., C. Pilskaln, M. Brzezinski, F. Lipschultz, M. Dennett, and G. B. Gardner. 1999. "Upward Transport of Oceanic Nitrate by Migrating Diatom Mats." *Nature* 397, no. 6718: 423–425. https://doi.org/10.1038/17103.

Waite, A. M., L. Stemmann, L. Guidi, et al. 2016. "The Wineglass Effect Shapes Particle Export to the Deep Ocean in Mesoscale Eddies." *Geophysical Research Letters* 43, no. 18: 9791–9800. https://doi.org/10.1002/2015gl066463.

Young, A. M., L. Karp-Boss, P. A. Jumars, and E. N. Landis. 2012. "Quantifying Diatom Aspirations: Mechanical Properties of Chain-Forming Species." *Limnology and Oceanography* 57, no. 6: 1789–1801. https://doi.org/10.4319/lo.2012.57.6.1789.

Supporting Information

Additional Supporting Information may be found in the online version of this article.

Submitted 08 May 2026
Revised 23 June 2026
Accepted 20 July 2026

Supplementary Tables and Figures for:

Giant phytoplankton revealed by in situ imaging

Mark D. Ohman, Karine Leblanc, Jeffrey S. Ellen, Sven Gastauer. 2026.

Limnology and Oceanography Letters 11, e70163 doi: 10.1002/lol2.70163

Suppl. Table S1. Locations of vertical phytonet sampling near water parcels transited by *Zooglider*.

Station	Date	Start Time	Latitude	Longitude
M	2 May 2023	13:59	39.494° N	4.091° E
M2	5 May 2023	13:13	39.671° N	3.958° E
B3	12 May2023	13:50	40.782° N	5.149° E

Suppl. Table S2. Maximum dimensions of phytoplankton chains after net collection and measurement in the laboratory. Taxa highlighted in blue were found to be abundant or dominant in SEM samples but not light microscopy samples. Taxa are listed in approximate order of relative abundance at each station. (*Long chains were not observed, so an assumption of a maximum of 20 cells per chain was made for maximal length estimates, based on individual cell dimensions.)

Station	Taxon	Maximum Length (mm)
M	*Stephanopyxis cf. palmeriana*	0.6
	Chaetoceros spp.	0.3
	Hemiaulus hauckii	0.24
	Thalassiothrix	1.7
	Pseudo-nitzschia cf. seriata	0.4
	Rhizosolenia styliformis	0.6
	Proboscia	1.7
	Delphineis minutissima	0.08*
	Lauderia annulata	0.12*
M2	*Chaetoceros* spp.	0.2
	Chaetoceros cf. peruvianus	0.2
	Thalassiothrix	1.7
	Thalassionema nitzschioides	0.36
	Hemiaulus hauckii	0.29
	Rhizosolenia styliformis	1.3
	Pseudosolenia calcar-avis	0.63
	Pseudo-nitzschia cf. *seriata*	0.64
	Proboscia alata	0.5
	Proboscia	1.7
	Detonula pumila	0.68
	Lauderia annulata	0.58
	Stephanopyxis	1.5*
	Leptocylindrus	1.8*
	Trichodesmium	0.73
	Detonula pumila	0.25*
B3	*Hemiaulus*	0.24
	Proboscia alata	> 0.58
	Leptocylindrus mediterraneus	0.4
	Chaetoceros dadayi	0.36
	Rhizosolenia	1.15

Guinardia striata	0.4
Guinardia flaccida (1 cell)	0.18
Pseudo-nitzschia	1.5*
Trichodesmium	0.45
Bacteriastrum	0.45*

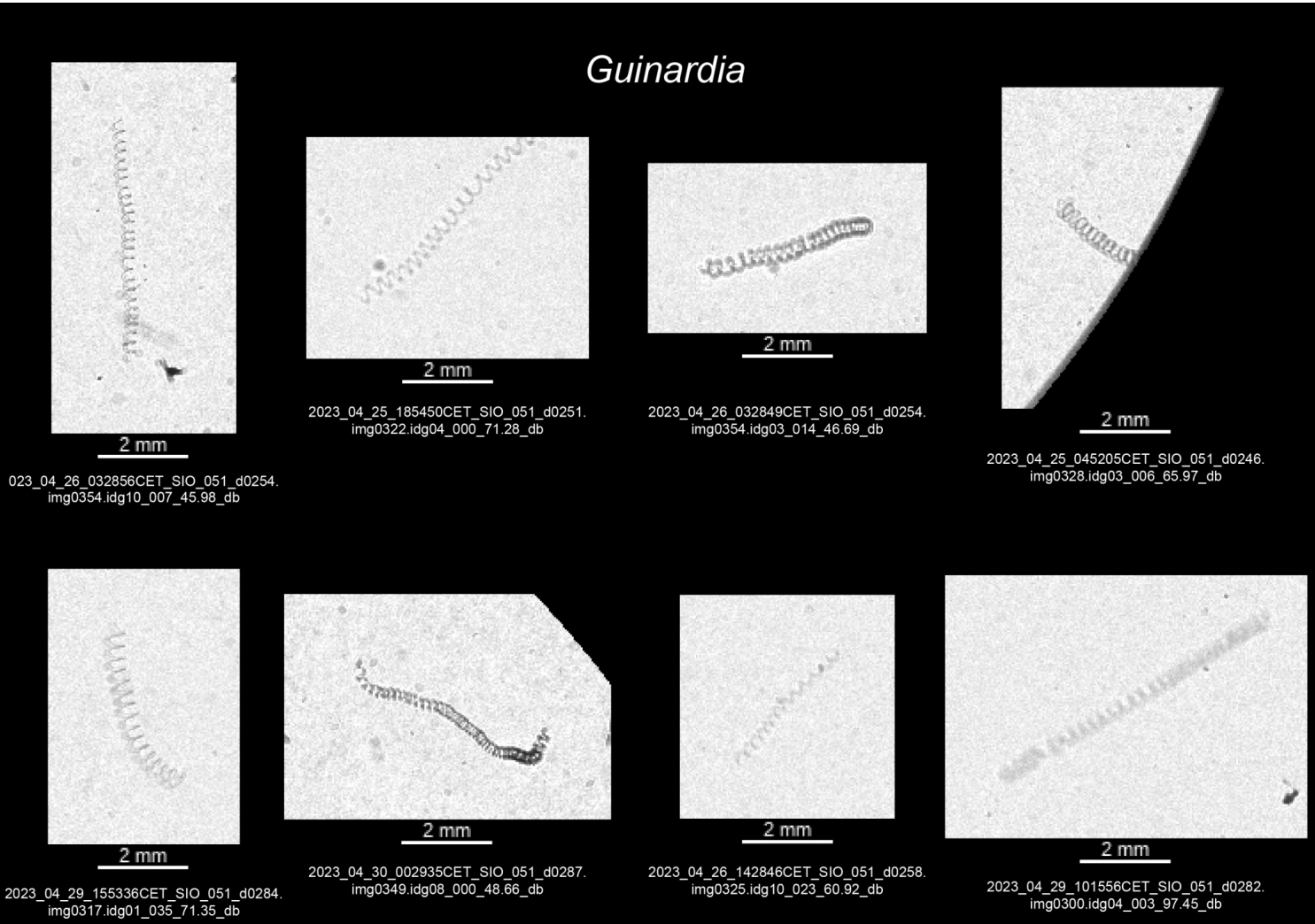

Fig. S1. Examples of *Guinardia* spp. imaged in situ by *Zooglider* in the BioSWOT-Med region. Image metadata are indicated beneath each image (date, local time, mission number, dive number, image number, sampling depth as pressure in dbar).

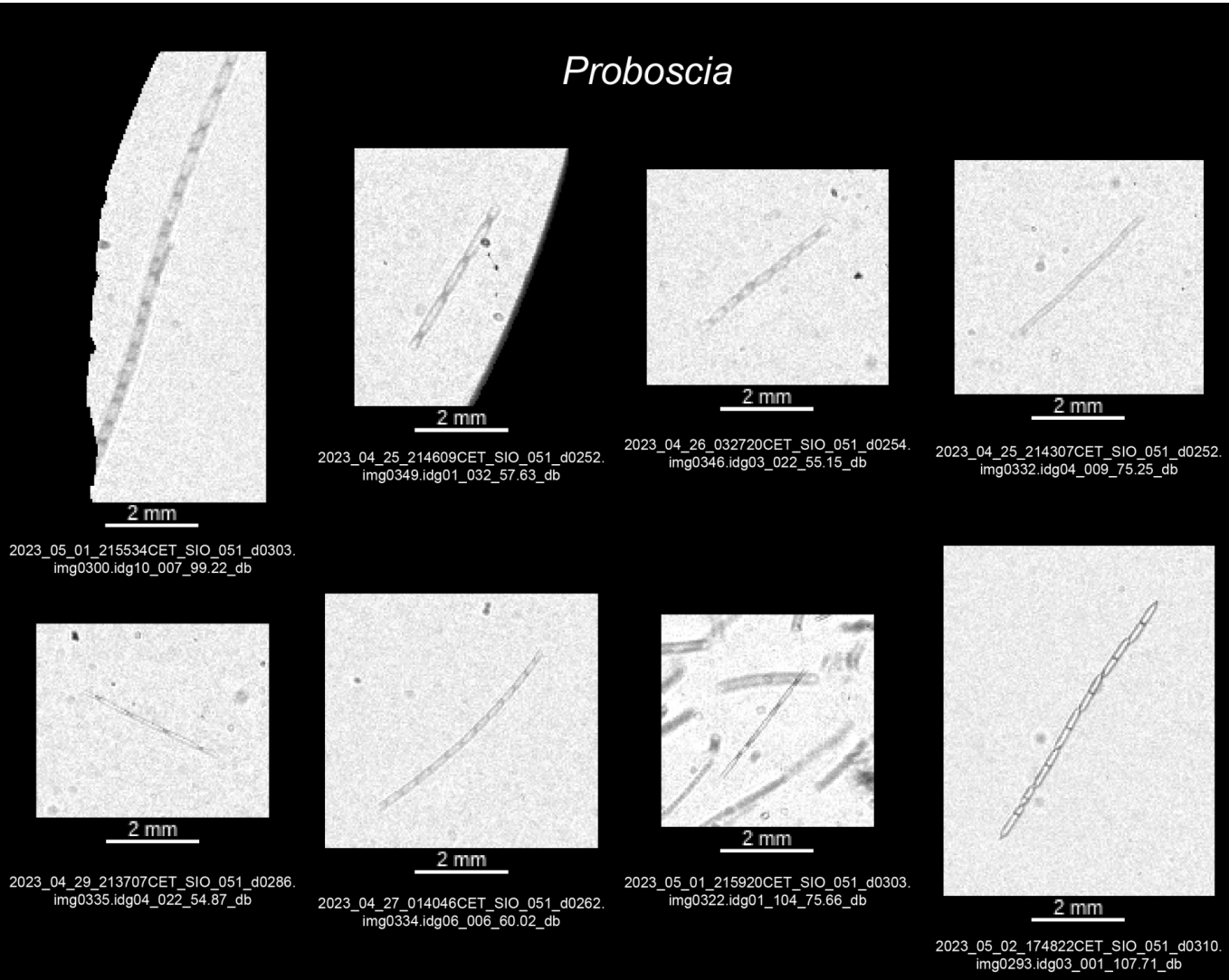

Fig. S2. Examples of *Proboscia* spp. imaged in situ by *Zooglider* in the BioSWOT-Med region. Metadata as in Fig. S1.

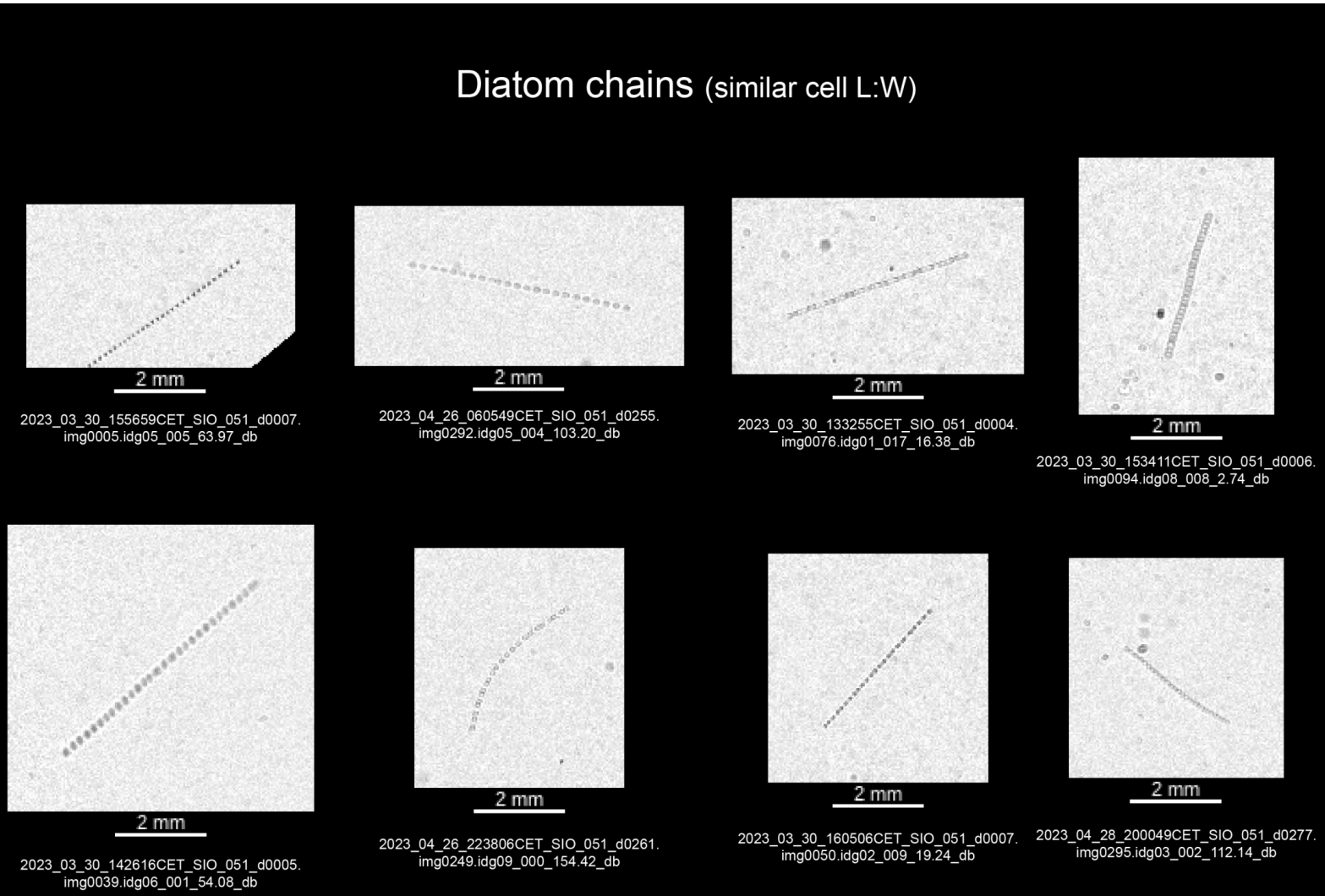

Fig. S3. Examples of Diatom chains with similar cell Length:Width imaged in situ by *Zooglider* in the BioSWOT-Med region. Metadata as in Fig. S1.

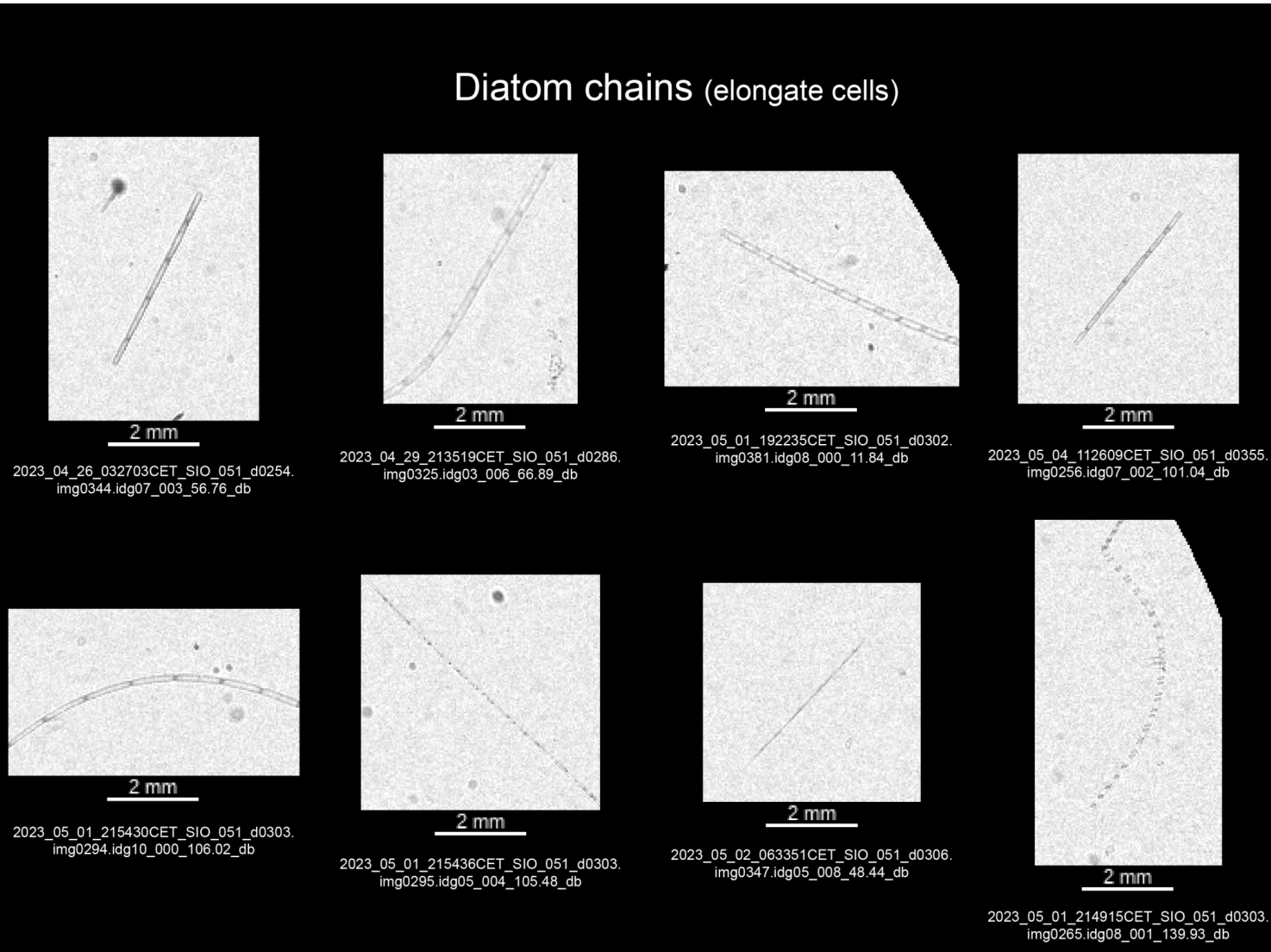

Fig. S4. Examples of Diatom chains with elongate cells imaged in situ by *Zooglider* in the BioSWOT-Med region. Metadata as in Fig. S1.

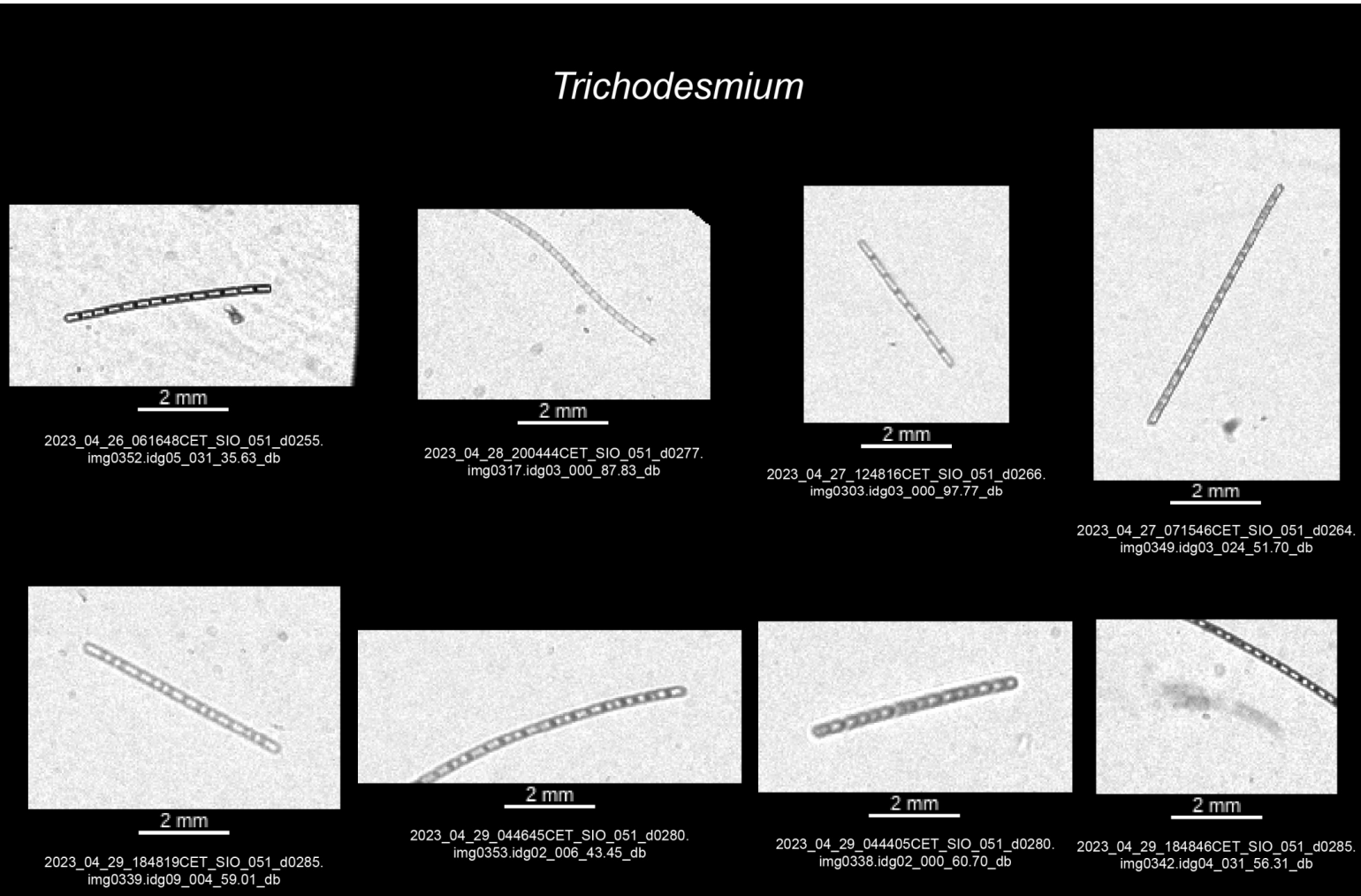

Fig. S5. Examples of *Trichodesmium* imaged in situ by *Zooglider* in the BioSWOT-Med region. Metadata as in Fig. S1.

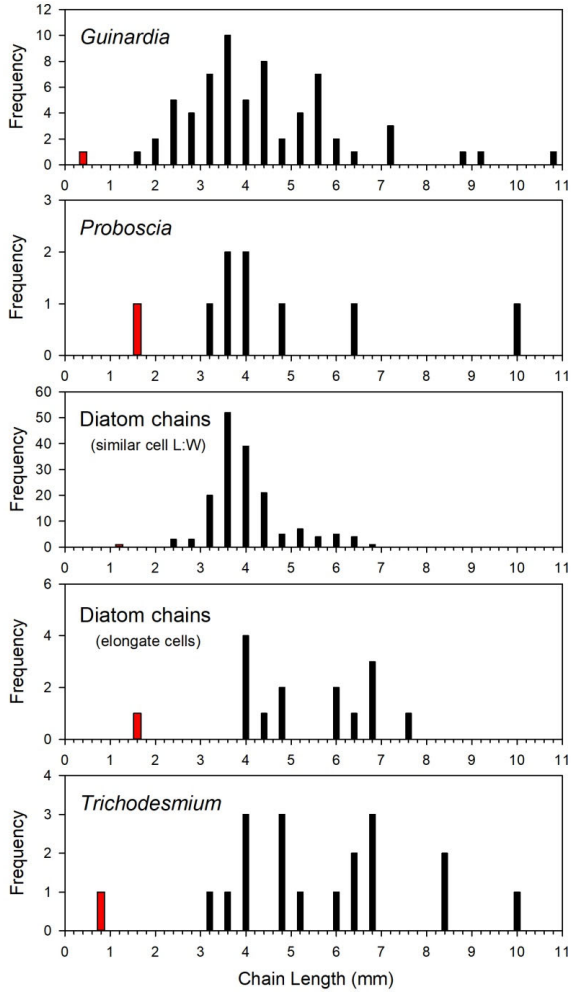

Fig. S6. Size frequency distribution of each of the five types of phytoplankton chains imaged in situ by *Zooglider* in the BioSWOT-Med region (black bars). Red bars indicate the largest corresponding chain measured in net-collected samples in the laboratory.